Bioactive Gyroid Scaffolds Formed by Sacrificial Templating of Nanocellulose and Nanochitin Hydrogels as Instructive Platforms for Biomimetic Tissue Engineering

WILEY-VCH

DOI: 10.1002/((please add manuscript number))
Article type: Communication

Bioactive Gyroid Scaffolds Formed by Sacrificial Templating of Nanocellulose and Nanochitin Hydrogels as Instructive Platforms for Biomimetic Tissue Engineering

Jose Guillermo Torres-Rendon, Tim Femmer, Laura De Laporte, Thomas Tigges, Khoshrow Rahimi, Felix Gremse, Sara Zafarnia, Wiltrud Lederle, Shinsuke Ifuku, Matthias Wessling, John G. Hardy, Andreas Walther**

J. G. Torres-Rendon, T. Femmer, Dr. L. De Laporte, T. Tigges, K. Rahimi, Prof. Dr. M. Wessling, Dr. A. Walther
DWI – Leibniz-Institute for Interactive Materials, RWTH Aachen University, Forckenbeckstr. 50, D-52056 Aachen, Germany
E-mail: walther@dwi.rwth-aachen.de

T. Femmer, Prof. Dr. M. Wessling
Chemical Process Engineering AVT.CVT, RWTH Aachen University, Turmstr. 46, D-52064 Aachen, Germany

F. Gremse, S. Zafarnia, Dr. W. Lederle
Department of Experimental Molecular Imaging, Medical Faculty, RWTH Aachen University, Pauwelsstr. 30, D-52074 Aachen, Germany

Prof. Dr. S. Ifuku
Graduate School of Engineering, Tottori University, 101-4 Koyama-cho Minami, Tottori, 680-8502, Japan

Dr. J. G. Hardy
School of Pharmacy, Medical Biology Centre, Queen's University Belfast, 97 Lisburn Road, Belfast BT9 7BL, Northern Ireland
E-mail: johnhardyuk@gmail.com

Keywords: stem cells, cellulose nanofibrils, chitin nanofibrils, 3D printing, hydrogel scaffolds

Biological tissues are hierarchical composite materials with tissue-specific chemical, mechanical and topographical properties. The development of biomimetic materials containing similarly structured features organized on vastly different length scales remains very challenging in materials science and engineering. For instance, hierarchical self-assembly of nanoscale building blocks into structures with highly ordered micrometer or even millimeter-scale periodicities is difficult to achieve.[1] Nature's solution to this problem is slow controlled growth, coupled with the inherent ability of natural tissues to remodel themselves, enabling tissue development and the repair of defects. One example of such hierarchical tissues is bone, comprising ordered macropores while at the same time having a hierarchically ordered nano- and mesostructure built up from aligned collagen fibrils and hydroxyl apatite nanoparticles.[2, 3]

In the synthetic world, ordered porous structures are important for a range of technologies, including batteries, meta-materials, photonics, sensors, and moreover as 3D scaffolds for fundamental biological studies, tissue engineering and regenerative medicine.[4-10] Chemical modifications or the incorporation of nanostructural features may enhance the properties of such 3D materials. This also involves advanced generative manufacturing techniques able to integrate top-down structuring processes with well-organized nanoscale building blocks and self-assembly to bridge structural length scales from nano-to-macro. In the context of 3D scaffolds for fundamental biological studies, tissue engineering and regenerative medicine, it remains a challenging task to develop simple and versatile pathways to impart biomimetic topographical features into hydrogel-based biomaterials. Topographical control is important for cell alignment (or migration) as clearly observable within the aligned pores in bone, cardiac, nerve and other tissues.[11] Therefore, the development of biomaterials, mimicking these topographically complex tissues that may instruct the behavior of cells inhabiting the scaffolds, is of great interest.[2, 7, 9, 12-18] Additional layers of complexity can be engineered into such materials through chemical patterning to bestow instructive chemical cues to which

cells respond,[19-23] and tailoring the mechanical properties of the underlying building blocks, which has enabled the control of cell behavior (including stem cell differentiation).[15, 24-26] In this respect, hydrogels based on self-assembling biomolecules or nanofibrils are attractive due to their ease of chemical modification, advanced and tunable mechanical properties, as well as the possible mesoscale alignment of such colloidal scale nanofibrils to guide cell alignment.[27, 28]

Consequently, the development of porous hydrogel-based tissue scaffolds has attracted great attention in recent years. Sacrificial templates are commonly used to impart porosity to gels, for example, removal of particles embedded within a polymer matrix may produce foams with randomly distributed interconnected pores,[13] whereas the removal of colloidal crystals yields inverse opals with well-defined pore interconnectivity.[14] Although such approaches are appealing because they are cheap and scalable, lithographic procedures and rapid prototyping techniques offer much greater versatility in terms of accessible topographies, defect/patient-specific geometries, and importantly facilitate the generation of asymmetric and/or anisotropic geometries that mimic natural tissues.[7, 9, 16] The dimensional resolution and preparation speed of these methods have an inverse relationship: 2-photon lithography provides the best resolution for the most complex geometries,[19, 29] but suffers from slow writing speed, which hampers the preparation of large geometries, whereas, classical nozzle extrusion in rapid prototyping is typically much faster albeit with a lower resolution.[12] The capabilities of digital light processing using MEMS technology and micromirrors to selectively irradiate voxels in a layered fashion provides intermediate capabilities. It combines freedom of geometrical design with attractive sub-millimeter size features and sufficient porosity for nutrient supply and the dissolution of waste metabolites during *in vitro* cell studies, as well as swift specimen production.[16, 17] One central bottleneck in generative manufacturing is the limited selection of suitable polymers (thermoplastics for extrusion) or photo-polymerizable resins. Moreover, such fabrication methods remain particularly difficult to combine with

sophisticated bottom-up self-assembled hydrogel materials, nanofibrils or self-assembling small molecules.

To overcome these obstacles we present a new reverse templating strategy towards ordered hydrogel scaffolds incorporating nanofibrillar building blocks. We use mathematically defined, cm-scale minimal surface architectures printed with sub-millimeter resolution by the micromirror technique as sacrificial templates and infiltrate them with nanofibrillar hydrogels. The sacrificial template contains labile crosslinks that facilitate their complete dissolution yielding hydrogel replicas with *de novo* designed pore structures (Scheme 1a-d). This simple approach represents a platform fabrication method for a range of hydrogel-based materials. We focus on hydrogels formed by renewable, high aspect ratio cellulose and chitin nanofibrils (CNF, ChNF, length = 0.1 – 5 μm, diameter = 2 – 5 nm, density, δ, = 1.01 g mL^{-1}). While porous tissue scaffolds with *de novo* designed biomimetic topographies are broadly applicable in soft/hard tissue engineering, we apply the materials to bone tissue engineering. We show that human mesenchymal stem cells (HMSCs) adhere to the scaffolds and, moreover, that additional chemical information programmed into the scaffolds (i.e., a collagen-mimetic coating with calcium phosphate) acts as an instructional cue inducing differentiation towards osteogenic outcomes.

We first focus on the preparation of the sacrificial templates. The resin used for the step-wise lithographic 3D printing of the sacrificial templates is adapted from a previous report[30] and based on a mixture of methacrylates and acrylamides, and contains methacrylic anhydride as a hydrolytically labile crosslinker. This resin is simple to prepare and allows features of ~ 50 μm with an aspect ratio of 1 to be printed with a precision better than 1 μm. We prepared two differently sized cubic templates with gyroid geometries containing 50 vol% of solid material and edge lengths of 10 and 15 mm (Scheme 1e, Figure 1a, Table S1). Both contain 6x6x6 unit cells, and the smaller cube is prepared close to the resolution limit of the instrument. Such minimal surface structures are topographically interesting for tissue scaffolds, as they provide

two bicontinuous interpenetrating volumes connected by 4-fold junction points allowing for sufficient nutrient supply and waste dissolution, and providing high surface areas and mechanical robustness.[16, 17] *In vivo*, the porosity of bones varies very widely from ca. 3.5% for cortical canals to ca. 80% in trabecular bone,[31, 32] therefore, the development of scaffolds with porosities of ca. 50% would conceptually be applicable to bone tissue engineering. The printing proceeds with a near perfect reproduction of the CAD model into the printed material, as further characterized with X-ray microcomputed tomography (µCT; Scheme 1e, Figure 1a,e). Additional scanning electron microscopy (SEM, Supporting Information (SI), Figure S1) reveals the layers of the stepwise lithography.

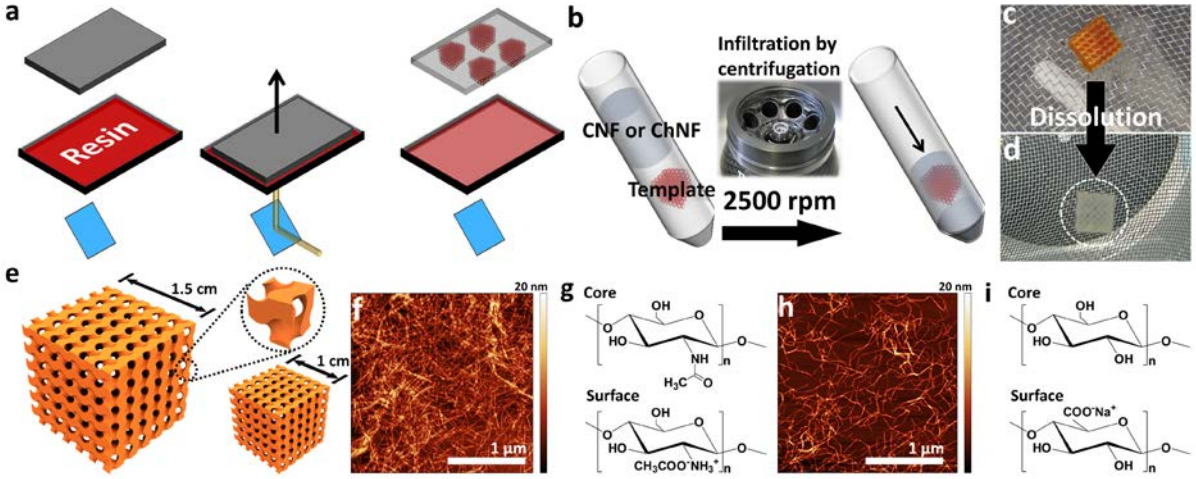

Scheme 1. Preparation of sacrificial templates, and reverse templating of hydrogel scaffolds based on cellulose and chitin nanofibrils. (a-d) Preparation of the gyroid sacrificial templates by layered micromirror lithography, followed by filling the void space with nanofibrillar hydrogels and subsequent dissolution of the sacrificial template in alkaline media. (e) Scaffold structure and dimensions. AFM images and chemical structures on the surface and in the core of ChNF (f, g) and CNF (h, i) nanofibrils.

We fill the void space of the templates with gel-like dispersions of cellulose and chitin nanofibrils in water (CNF, ChNF; 1 wt%, Scheme 1f-i). These nanofibrils are typically isolated from wood and crustaceans by chemical or enzymatic pretreatment in water and subsequent mechanical homogenization. Such globally abundant and renewable resources are

sustainable feedstocks and certain to be a mainstay of the forthcoming green materials revolution.[33-36] Most importantly, the highly crystalline character of the nanofibrils is preserved during the extraction and yields nanofibrils of two of the stiffest natural materials ($E_{\alpha\text{-}chitin}$ = 41-60 GPa; $E_{cellulose\text{-}I}$ = 138 GPa).[37-39] We use TEMPO-oxidized anionic CNF and surface-deacetylated cationic ChNF. Atomic force microscopy (AFM) reveals well-defined nanofibrils with micrometer lengths and average diameters of 2.5 ± 2 nm and 3.2 ± 1.1 nm for CNF and ChNF (Scheme 1f-i; see SI for an exhaustive characterization). They are interesting building blocks for cell studies as they provide a stiff microenvironment for the mechanosensation of cells, thus complementing polymeric hydrogels.

These nanofibrils were previously used to prepare transparent nanopapers,[40-42] nanocomposites[43, 44] and fibers[45-47] with outstanding mechanical and functional properties.[48, 49] Both nanofibrils form hydrogels at 1 wt%[36] with shear thinning and self-mending behavior, allowing filling of the sacrificial templates simply by centrifugation. After removal of excess hydrogel the gel-filled template is placed into 1 wt% NaOH to dissolve the sacrificial resin template, a process that is swifter in alkaline media. The resulting porous hydrogel scaffolds shown in Scheme 1d can be readily handled with blunt tweezers. Interestingly, even anionic CNFs can be templated with this method, despite the fact that they are normally easily dispersed in alkaline water. The interfibrillar hydrogen bonds, interfibrillar entanglements and ionic strength maintain the integrity of the templated scaffold during extraction of the sacrificial template. We assured the persistence of the crystalline nature of the nanofibrils by X-ray diffraction of the scaffolds, which yields degrees of crystallinity of 63 % and 70 % for CNF and ChNF, respectively (Figure S2). The final scaffolds are stable in water for more than a year and do not lose their shape.

Photographs of the scaffolds (Figure 1b,d,f,g) demonstrate how well the macroscopic template structure can be transferred into the nanofibrillar hydrogels, and SEM imaging after supercritical drying shows both the macropores imparted by the lithography and the

nanopores arising from the nanofibril network (Figure 1i-k). Using a theoretical model for nanofibrillar networks,[50] it is possible to calculate the average pore radius of the hydrogels to ca. 20 and 26 nm for 1 wt% dispersions of CNF and ChNF, respectively (details in Supplementary Note 1). This length scale corresponds well to the average pore radius of ca. 14 nm determined by statistical image analysis of a supercritically dried CNF scaffold (Figure S3). This pore size in the hydrogel is sufficient to allow nutrient diffusion, and also potentially allows intercellular communication through the matrix in more complex geometries. Supercritical drying is not mandatory to transfer the scaffolds into a new medium as they readily recover their shapes after air drying and re-exposure to water, making the handling very easy (Figure 1b,c,g). The interesting shape recovery properties are due to the stiffness of the nanofibrils and that drying reinforces the interfibrillar hydrogen bonds which leads to a build-up of internal stress during the collapse of the macropores that is released upon rehydration, resulting in shape recovery.

The accuracy of the sacrificial templating process is high, with differences in size between the original CAD model and the hydrogel scaffold of less than 15% for CNF or 5% for ChNF as determined by imaging. A direct µCT of supercritically dried scaffolds is not possible due to the low mass fraction of the nanofibrils (1 wt% in hydrogel, $\delta_{\text{supercritically-dried}} \approx 0.01$ g mL^{-1}), yet the addition of 1 wt% $BaSO_4$ microparticles into the hydrogel allows µCT imaging, potentially enabling their visualization *in vivo* (Figure 1h). Confocal fluorescence imaging of the surface of the hydrated ChNF scaffolds labeled with fluorescein isothiocyanate (FITC) shows a low micron-scale roughness (Figure 1l).

The incorporation of $BaSO_4$ demonstrates that large quantities of inorganics or carriers can be added to the hydrogels. We subsequently employ this feature to impart biomimetic chemical properties to the scaffolds to facilitate the differentiation of human mesenchymal stem cells (HMSCs). FITC-labeling demonstrates the accessibility of the amines in ChNF-scaffolds for covalent modification that may facilitate tuning of their degradation/mechanical properties via

crosslinking, or their biochemical properties via incorporation of cell-adhesive peptides or other biological epitopes in the future.

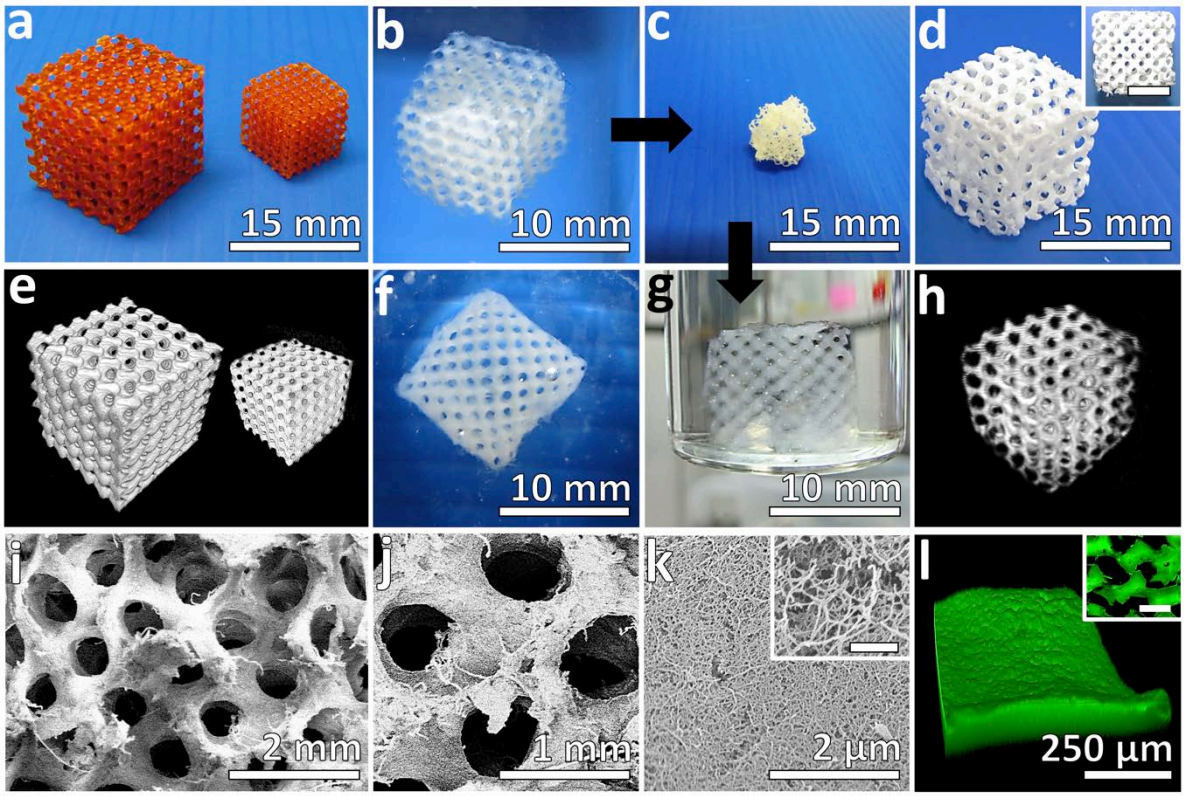

Figure 1. Multiscale structural characterization and shape recovery behavior. Photographs of (a) the templates and (e) their µCT structures. (b,f) Photographs of CNF and ChNF scaffolds with 10 mm edge length. (b,c,g) Shape recovery behavior of a CNF scaffold. (d) Photographs of a cubic scaffold with 15 mm edge lengths after supercritical drying. The scale bar in the inset is 8 mm. (h) µCT structure of a ChNF scaffold with 10 mm edge length containing 1 wt% $BaSO_4$. (i-k) SEM images of a ChNF scaffold with 10 mm edge length at different magnifications (scale bar in inset of (k) is 250 nm). (l) 3D reconstruction of the surface of a ChNF hydrogel scaffold using confocal fluorescence imaging after staining with FITC. The inset shows a 2D slice with a scale bar of 1 mm.

We believe that our simple process of replica formation based on lithographically produced sacrificial templates is widely applicable to the formation of hard/soft tissue scaffolds. This will give rise to *de novo* designed biomimetic topographies based on a variety of delicate hydrogel-forming materials, including supramolecular structures, such as self-assembling peptides, DNA or block copolymer hydrogels. The main prerequisite at this point is the stability of the structures in mildly basic solution, which can in most cases be achieved by

appropriate molecular design. We foresee that the adaptation of the chemistry underlying the sacrificial templates will enable their removal using different conditions (temperatures, solutions or non-aqueous solvents) further broadening the applicability and appeal of this concept.

With a view to demonstrating such scaffolds function as instructive platforms for tissue engineering, we sought to use them as biomimetic scaffolds for bone tissue engineering. Pertinently, polysaccharide-based biomaterials are interesting because they tend to display low immunogenicity when implanted *in vivo*[51, 52]. A structural analogue, bacterial cellulose, which is very difficult to process into complex 3D shapes, has shown promising results for simpler 3D structures such as artificial blood vessels/vascular grafts for bone[53] and cartilage[54] regeneration. CNF hydrogels support the adhesion and proliferation of human liver cells (HepG2 and HepaRG),[55, 56] human pluripotent stem cells (hPSCs),[57] and mouse fibroblasts (NIH-3T3).[58] ChNF-based materials support the adhesion and proliferation of mouse and human fibroblasts, keratinocytes and epithelial cells *in vitro*.[59-61] In addition, both materials are complementary with respect to *in vivo* degradation. Chitin and also chitosan materials are known to undergo *in vivo* degradation.[51] By comparison, cellulose-based materials are considered biodurable, however, the addition of cytocompatible cellulose-degrading enzymes (i.e., cellulase) has been suggested as means to degrade cellulose *in vivo* and produce glucose as nutrient byproduct.[62, 63]

We examined basic biocompatibility and differences in cell proliferation on 2D surfaces of the materials via an MTS proliferation assay using widely available mouse fibroblasts, which are ubiquitous in the body (in skin, peripheral nerves, muscles and indeed bone marrow tissues, Figure S4). The proliferation assay demonstrates growth on CNF surfaces, comparable to normal tissue culture polystyrene, whereas the growth is significantly lower on ChNF surfaces and slows down after 48 hours.

To investigate their efficacy as instructive bone tissue scaffolds, we proceeded to investigate the interaction of HMSCs with our hydrogel-based materials. We initiated our studies with simple 2D films, observing marked differences in the propensity of the HMSCs to adhere to the different nanofibrils. While HMSCs adhere and spread on CNF, adhesion to ChNF is poor (Figure 2a,c,e,g), which reflects the MTS proliferation data of mouse fibroblasts. This behavior can be explained considering cell adhesion to biomaterials, which depends on the distribution of different proteins that adsorb on the surface of a biomaterial. Under physiologically-mimetic conditions, i.e. PBS at pH 7.4, the carboxyl groups of CNF are deprotonated and therefore negatively charged. Collagen-1 is one of the most important proteins governing cell adhesion and the isoelectric point of collagen-1 is ca. 8.3, hence it is positively charged at pH 7.4.[64] Consequently, we postulate that collagen adsorption on CNF surfaces mediated by electrostatic interactions aids cell adhesion. In case of chitin and chitosan (deacetylated chitin), it has been reported that both types have both inhibitory and stimulatory effects on cells *in vitro*,[65, 66] which are attributed to the different chemical composition, particularly the degree of deacetylation.[67] Human fibroblast adhesion to chitin with low degrees of deacetylation is poor,[68] whereas, human fibroblast and keratinocyte adhesion to highly deacetylated chitin (i.e. $\geq$ ca. 50%) is strong.[68, 69] We relate our observation of poor cell attachment (HSMCs) and slower proliferation (fibroblasts) to the low degree of deacetylation (ca. 10%) of our ChNF.

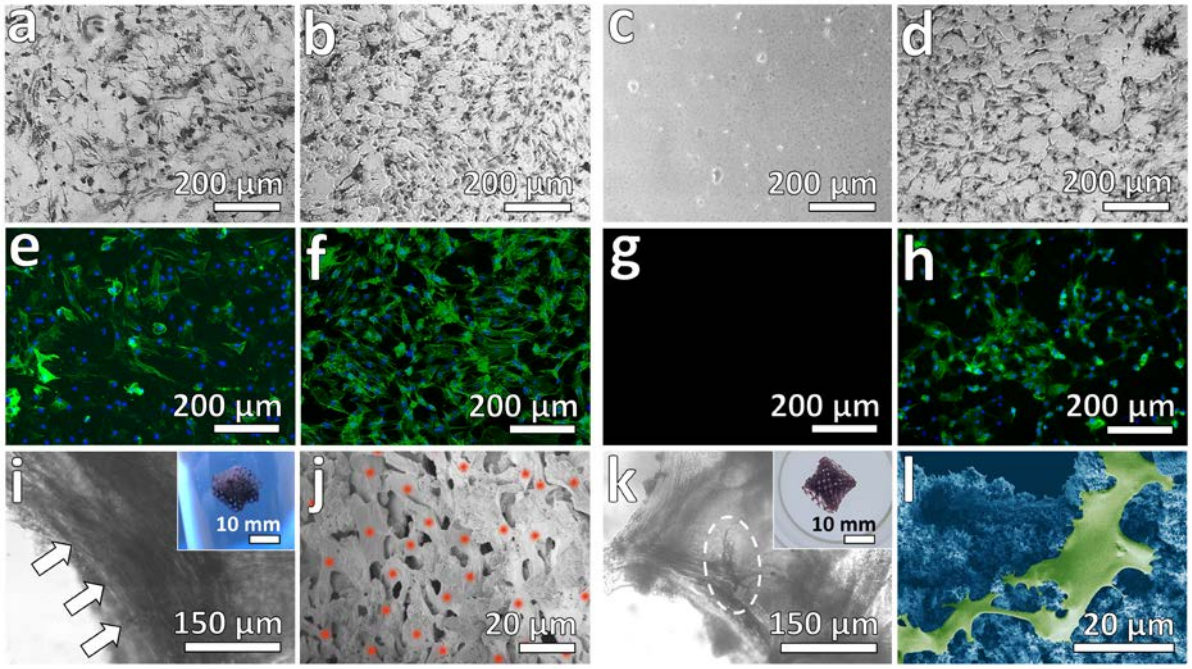

Figure 2. Microscopic characterization of HMSCs cultured on 2D films (a-h) and 3D gyroid scaffolds: (a-d) Bright-field microscopy after ALP live staining and (e-h) fluorescence microscopy after staining the actin filaments with Alexa Fluor 488 Phalloidin (green) and nuclei with DAPI (blue) of CNF films (a,e), CNF-Gel-$CaPO_4$ films (b,f), ChNF films (c,g) and ChNF-Gel-$CaPO_4$ films (d,h). (i,k) Bright-field microscopy after ALP live staining of CNF-Gel-$CaPO_4$ and ChNF-Gel-$CaPO_4$ scaffolds after sectioning to 1 mm thickness (insets show the homogeneous ALP live stain in the scaffolds; scale bars 10 mm). (j-l) SEM micrographs of a confluent cell layer in a CNF-Gel-CaPO4 scaffold (j, cell centers marked by red dots, see also Figure SI7) and well adherent HSMCs on a less densely populated area of the ChNF-Gel-$CaPO_4$ scaffold (l, false colored).

With a view to the application of the materials for bone tissue engineering, we deposited a cell adhesive collagen-mimetic coating (composed of a thiolated gelatin derivative that self-crosslinks upon exposure to air)[70] and thereafter a coating of calcium phosphate that would act as an ion source for the HMSCs to convert to hydroxyl apatite. Attachment of HMSCs is indeed significantly higher for the coated films (Gel-$CaPO_4$) compared to films of ChNF and CNF alone, demonstrating the benefit of a collagen-mimetic coating. In the case of films of CNF-Gel-$CaPO_4$, the average number of cells attached to the films increases by ca. 130 % compared to pristine CNF films (Figure S5). Furthermore, we observe that the chemical information programmed into the scaffolds acts as a cue to which HMSCs cultured on the

materials respond to by differentiation towards osteogenic outcomes as confirmed using a qualitative alkaline phosphatase (ALP) live stain (Figure 2a-d) and a quantitative ALP assay (Figure S6).

Importantly, HMSCs behave similarly on the 3D scaffolds coated with the gelatin derivative and calcium phosphate, and differentiate towards osteogenic outcomes (Figure S6). The ALP live stain shows that the cells are alive, functional and homogeneously distributed throughout the scaffolds, as seen by the homogeneous coloration (Figure 2, insets in i and k, Figure S7, further data for fibroblasts in scaffolds is displayed in Figure S8). Optical and scanning electron microscopy confirm that the HSMCs are anchored and spread within the biomimetic 3D environment provided by the hydrogel matrix (Figure 2i-l), thereby confirming the suitability of the gyroidal hydrogel scaffolds as substrates for biomimetic tissue engineering.

In summary, we demonstrate significant progress in two complementary directions. First we introduced a simple and straightforward way to make topographically complex hydrogels with mathematically defined pore geometries via a simple reverse templating approach and showcased the applicability of this methodology to structure gyroidal hydrogel scaffolds based on cellulose and chitin nanofibrils. We believe that this templating strategy will be widely applicable to other soft hydrogel materials including self-assembling peptides, peptide amphiphiles, silk proteins, collagen matrices, or for the enzymatic and chemical polymerization of hydrogel materials already optimized for soft tissue engineering. Secondly, we established important differences in terms of cell attachment of HSMCs on the surfaces of chitin vs. cellulose nanofibrils. Providing appropriate chemical cues via coating with a collagen-rich bone mimetic coating facilitates attachment of the HMSCs to both underlying polysaccharide nanofibrils and moreover encourages their differentiation towards osteogenic outcomes. We believe that this approach opens doors to produce complex topologies on demand by combining the capabilities of top-down generative manufacturing techniques (micro-to-macro structure) and increasingly complex soft hydrogel materials (nano-to-

mesostructure) bottom-up to allow for advanced and personalized biomimetic tissue engineering.

Experimental Section

Please see Supporting Information.

Supporting Information

Supporting Information (exp. section, calculation of the pore size, additional SEM, optical microscopy, XRD, MTS assay, cell count, ALP assay) is available from the Wiley Online Library or from the author.

Acknowledgements

We thank B. Wang for the AFM measurements, A. Kühne for initial confocal fluorescence microscopy, Ingela Bjurhager for orienting µCT, S. Moli for supporting cell studies and S. Rütten for supercritical drying. We acknowledge the BMBF for funding the AQUAMAT research group and the "ERANET Woodwisdom Program" financed by the BMELV. This work was performed in part at the Center for Chemical Polymer Technology CPT, which is supported by the EU and the federal state of North Rhine-Westphalia (grant no. EFRE 30 00 883 02). M.W. acknowledges the support of the Alexander-von-Humboldt Foundation. A.W. gratefully acknowledges continuous support from Martin Möller.

Received:
Revised:
Published online:

References

[1] P. Ke, X.-N. Jiao, X.-H. Ge, W.-M. Xiao, B. Yu, *R. Soc. Chem. Adv.* **2014**, 4, 39704.

[2] M. A. Meyers, P.-Y. Chen, A. Y.-M. Lin, Y. Seki, *Prog. Mater Sci.* **2008**, 53, 1.

[3] M. R. Rogel, H. Qiu, G. A. Ameer, *J. Mater. Chem.* **2008**, 18, 4233.

[4] N. Li, Z. Chen, W. Ren, F. Li, H.-M. Cheng, *Proc. Natl. Acad. Sci. U.S.A.* **2012**, 109, 17360.

[5] C. I. Aguirre, E. Reguera, A. Stein, *Adv. Funct. Mater.* **2010**, 20, 2565.

[6] J.-H. Lee, J. P. Singer, E. L. Thomas, *Adv. Mater.* **2012**, 24, 4782.

[7] S. J. Hollister, *Nat. Mater.* **2005**, 4, 518.

[8] M. E. Davis, *Nature* **2002**, 417, 813.

[9] J. L. Drury, D. J. Mooney, *Biomaterials* **2003**, 24, 4337.

[10] L. E. Kreno, K. Leong, O. K. Farha, M. Allendorf, R. P. Van Duyne, J. T. Hupp, *Chem. Rev.* **2011**, 112, 1105.

[11] A. R. Nectow, M. E. Kilmer, D. L. Kaplan, *J. Biomed. Mater. Res. Part A* **2014**, 102, 420.

[12] N. Annabi, A. Tamayol, J. A. Uquillas, M. Akbari, L. E. Bertassoni, C. Cha, G. Camci-Unal, M. R. Dokmeci, N. A. Peppas, A. Khademhosseini, *Adv. Mater.* **2014**, 26, 85.

[13] H. Bäckdahl, M. Esguerra, D. Delbro, B. Risberg, P. Gatenholm, *J. Tissue Eng. Regen. Med.* **2008**, 2, 320.

[14] S.-W. Choi, J. Xie, Y. Xia, *Adv. Mater.* **2009**, 21, 2997.

[15] D. E. Discher, D. J. Mooney, P. W. Zandstra, *Science* **2009**, 324, 1673.

[16] S. C. Kapfer, S. T. Hyde, K. Mecke, C. H. Arns, G. E. Schröder-Turk, *Biomaterials* **2011**, 32, 6875.

[17] F. P. W. Melchels, K. Bertoldi, R. Gabbrielli, A. H. Velders, J. Feijen, D. W. Grijpma, *Biomaterials* **2010**, 31, 6909.

[18] L. De Laporte, Y. Yang, M. L. Zelivyanskaya, B. J. Cummings, A. J. Anderson, L. D. Shea, *Mol. Ther.* **2008**, 17, 318.

[19] B. Richter, T. Pauloehrl, J. Kaschke, D. Fichtner, J. Fischer, A. M. Greiner, D. Wedlich, M. Wegener, G. Delaittre, C. Barner-Kowollik, M. Bastmeyer, *Adv. Mater.* **2013**, 25, 6117.

[20] A. S. Quick, J. Fischer, B. Richter, T. Pauloehrl, V. Trouillet, M. Wegener, C. Barner-Kowollik, *Macromol. Rapid Commun.* **2013**, 34, 335.

[21] T. Pauloehrl, G. Delaittre, M. Bruns, M. Meißler, H. G. Börner, M. Bastmeyer, C. Barner-Kowollik, *Angew. Chem. Int. Ed.* **2012**, 51, 9181.

[22] A. S. Quick, H. Rothfuss, A. Welle, B. Richter, J. Fischer, M. Wegener, C. Barner-Kowollik, *Adv. Funct. Mater.* **2014**, 24, 3571.

[23] J. C. Culver, J. C. Hoffmann, R. A. Poché, J. H. Slater, J. L. West, M. E. Dickinson, *Adv. Mater.* **2012**, 24, 2344.

[24] A. J. Engler, S. Sen, H. L. Sweeney, D. E. Discher, *Cell* **2006**, 126, 677.

[25] D. E. Discher, P. Janmey, Y.-l. Wang, *Science* **2005**, 310, 1139.

[26] G. C. Reilly, A. J. Engler, *J. Biomech.* **2010**, 43, 55.

[27] J. B. Matson, S. I. Stupp, *Chem. Commun.* **2012**, 48, 26.

[28] S. Maude, E. Ingham, A. Aggeli, *Nanomedicine* **2013**, 8, 823.

[29] T. Watanabe, M. Akiyama, K. Totani, S. M. Kuebler, F. Stellacci, W. Wenseleers, K. Braun, S. R. Marder, J. W. Perry, *Adv. Funct. Mater.* **2002**, 12, 611.

[30] R. Liska, F. Schwager, C. Maier, R. Cano-Vives, J. Stampfl, *J. Appl. Polym. Sci.* **2005**, 97, 2286.

[31] G. A. P. Renders, L. Mulder, L. J. Van Ruijven, T. M. G. J. Van Eijden, *J. Anat.* **2007**, 210, 239.

[32] L. Cardoso, S. P. Fritton, G. Gailani, M. Benalla, S. C. Cowin, *J. Biomech.* **2013**, 46, 253.

[33] S. Ifuku, M. Nogi, K. Abe, M. Yoshioka, M. Morimoto, H. Saimoto, H. Yano, *Biomacromolecules* **2009**, 10, 1584.

[34] J. D. Goodrich, W. T. Winter, *Biomacromolecules* **2007**, 8, 252.

[35] T. Saito, Y. Nishiyama, J.-L. Putaux, M. Vignon, A. Isogai, *Biomacromolecules* **2006**, 7, 1687.

[36] M. Pääkkö, M. Ankerfors, H. Kosonen, A. Nykänen, S. Ahola, M. Österberg, J. Ruokolainen, J. Laine, P. T. Larsson, O. Ikkala, T. Lindström, *Biomacromolecules* **2007**, 8, 1934.

[37] Y. Ogawa, R. Hori, U.-J. Kim, M. Wada, *Carbohydr. Polym.* **2011**, 83, 1213.

[38] T. Nishino, R. Matsui, K. Nakamae, *J. Polym. Sci. Part B Polym. Phys.* **1999**, 37, 1191.

[39] I. Sakurada, Y. Nukushina, T. Ito, *J. Polym. Sci.* **1962**, 57, 651.

[40] A. J. Benítez, J. G. Torres-Rendon, M. Poutanen, A. Walther, *Biomacromolecules* **2013**, 14, 4497.

[41] H. Sehaqui, Q. Zhou, O. Ikkala, L. A. Berglund, *Biomacromolecules* **2011**, 12, 3638.

[42] S. Ifuku, S. Morooka, M. Morimoto, H. Saimoto, *Biomacromolecules* **2010**, 11, 1326.

[43] J. Jin, P. Hassanzadeh, G. Perotto, W. Sun, M. A. Brenckle, D. Kaplan, F. G. Omenetto, M. Rolandi, *Adv. Mater.* **2013**, 25, 4482.

[44] S. Ifuku, S. Morooka, A. N. Nakagaito, M. Morimoto, H. Saimoto, *Green Chem.* **2011**, 13, 1708.

[45] J. G. Torres-Rendon, F. H. Schacher, S. Ifuku, A. Walther, *Biomacromolecules* **2014**, 15, 2709.

[46] P. Das, T. Heuser, A. Wolf, B. Zhu, D. E. Demco, S. Ifuku, A. Walther, *Biomacromolecules* **2012**, 13, 4205.

[47] A. Walther, J. V. I. Timonen, I. Díez, A. Laukkanen, O. Ikkala, *Adv. Mater.* **2011**, 23, 2924.

[48] N. Zhao, Z. Wang, C. Cai, H. Shen, F. Liang, D. Wang, C. Wang, T. Zhu, J. Guo, Y. Wang, X. Liu, C. Duan, H. Wang, Y. Mao, X. Jia, H. Dong, X. Zhang, J. Xu, *Adv. Mater.* **2014**, 26, 6994.

[49] M. Wang, I. V. Anoshkin, A. G. Nasibulin, J. T. Korhonen, J. Seitsonen, J. Pere, E. I. Kauppinen, R. H. A. Ras, O. Ikkala, *Adv. Mater.* **2013**, 25, 2428.

[50] Nadine R. Lang, S. Münster, C. Metzner, P. Krauss, S. Schürmann, J. Lange, Katerina E. Aifantis, O. Friedrich, B. Fabry, *Biophys. J.* **2013**, 105, 1967.

[51] K. Tomihata, Y. Ikada, *Biomaterials* **1997**, 18, 567.

[52] N. Yanamala, M. T. Farcas, M. K. Hatfield, E. R. Kisin, V. E. Kagan, C. L. Geraci, A. A. Shvedova, *ACS Sustainable Chem. Eng.* **2014**, 2, 1691.

[53] S. Saska, H. S. Barud, A. M. M. Gaspar, R. Marchetto, S. J. L. Ribeiro, Y. Messaddeq, *Int. J. Biomater.* **2011**, 2011, 8.

[54] A. Svensson, E. Nicklasson, T. Harrah, B. Panilaitis, D. L. Kaplan, M. Brittberg, P. Gatenholm, *Biomaterials* **2005**, 26, 419.

[55] M. Bhattacharya, M. M. Malinen, P. Lauren, Y.-R. Lou, S. W. Kuisma, L. Kanninen, M. Lille, A. Corlu, C. GuGuen-Guillouzo, O. Ikkala, A. Laukkanen, A. Urtti, M. Yliperttula, *J. Control. Release* **2012**, 164, 291.

[56] M. M. Malinen, L. K. Kanninen, A. Corlu, H. M. Isoniemi, Y.-R. Lou, M. L. Yliperttula, A. O. Urtti, *Biomaterials* **2014**, 35, 5110.

[57] Y.-R. Lou, L. Kanninen, T. Kuisma, J. Niklander, L. A. Noon, D. Burks, A. Urtti, M. Yliperttula, *Stem Cells Dev.* **2013**, 23, 380.

[58] H. Cai, S. Sharma, W. Liu, W. Mu, W. Liu, X. Zhang, Y. Deng, *Biomacromolecules* **2014**, 15, 2540.

[59] M. Rolandi, R. Rolandi, *Adv. Colloid Interface Sci.* **2014**, 207, 216.

[60] I. Ito, T. Osaki, S. Ifuku, H. Saimoto, Y. Takamori, S. Kurozumi, T. Imagawa, K. Azuma, T. Tsuka, Y. Okamoto, S. Minami, *Carbohydr. Polym.* **2014**, 101, 464.

[61] H. K. Noh, S. W. Lee, J.-M. Kim, J.-E. Oh, K.-H. Kim, C.-P. Chung, S.-C. Choi, W. H. Park, B.-M. Min, *Biomaterials* **2006**, 27, 3934.

[62] A. Sannino, C. Demitri, M. Madaghiele, *Materials* **2009**, 2, 353.

[63] E. Entcheva, H. Bien, L. Yin, C.-Y. Chung, M. Farrell, Y. Kostov, *Biomaterials* **2004**, 25, 5753.

[64] J. Uquillas, O. Akkus, *Ann. Biomed. Eng.* **2012**, 40, 1641.

[65] L. Y. Chung, R. J. Schmidt, P. F. Hamlyn, B. F. Sagar, A. M. Andrew, T. D. Turner, *J. Biomed. Mater. Res.* **1994**, 28, 463.

[66] T. Mori, M. Okumura, M. Matsuura, K. Ueno, S. Tokura, Y. Okamoto, S. Minami, T. Fujinaga, *Biomaterials* **1997**, 18, 947.

[67] G. I. Howling, P. W. Dettmar, P. A. Goddard, F. C. Hampson, M. Dornish, E. J. Wood, *Biomaterials* **2001**, 22, 2959.

[68] S. B. Lee, Y. H. Kim, M. S. Chong, Y. M. Lee, *Biomaterials* **2004**, 25, 2309.

[69] C. Chatelet, O. Damour, A. Domard, *Biomaterials* **2001**, 22, 261.

[70] X. Z. Shu, Y. Liu, F. Palumbo, G. D. Prestwich, *Biomaterials* **2003**, 24, 3825.

TOC

Sacrificial templating using lithographically printed minimal surface structures allows complex *de novo* geometries of delicate hydrogel materials. The hydrogel scaffolds based on cellulose and chitin nanofibrils show differences in terms of attachment of human mesenchymal stem cells, and allow their differentiation into osteogenic outcomes. Our approach serves as a first example towards designer hydrogel scaffolds viable for biomimetic tissue engineering.

Keywords: stem cells, 3D printing, cellulose nanofibrils, chitin nanofibrils, hydrogel scaffolds

J. G. Torres-Rendon, T. Femmer, L. De Laporte, T. Tigges, K. Rahimi, F. Gremse, S. Zafarnia, W. Lederle, S. Ifuku, M. Wessling, J. G. Hardy,* A. Walther*

Title: Bioactive Gyroid Scaffolds Formed by Sacrificial Templating of Nanocellulose and Nanochitin Hydrogels as Instructive Platforms for Biomimetic Tissue Engineering